Transmission Techniques for Downlink Multi-Antenna MC-CDMA Systems in a Beyond-3G Context

Fabrice Portier, Ivana Raos, Adão Silva, Jean-Yves Baudais, Jean-François Hélard, Atílio Gameiro, and Santiago Zazo

Abstract: **The combination of multiple antennas and multi-carrier code division multiple-access (MC-CDMA) is a strong candidate for the downlink of the next generation mobile communications. The study of such systems in scenarios that model real-life transmissions is an additional step towards an optimized achievement. We consider a realistic MIMO channel with two or four transmit antennas and up to two receive antennas, and channel state information (CSI) mismatches. Depending on the mobile terminal (MT) class, its number of antennas or complexity allowed, different data-rates are proposed with turbo-coding and asymptotic spectral efficiencies from 1 to 4.5 bit/s/Hz, using three algorithms developed within the European IST-MATRICE project. These algorithms can be classified according to the degree of CSI at base-station (BS): *i*) Transmit space-frequency prefiltering based on constrained zero-forcing algorithm with complete CSI at BS; *ii*) transmit beamforming based on spatial correlation matrix estimation from partial CSI at BS; *iii*) orthogonal space-time block coding based on Alamouti scheme without CSI at BS. All presented schemes require a reasonable complexity at MT, and are compatible with a single-antenna receiver. A choice between these algorithms is proposed in order to significantly improve the performance of MC-CDMA and to cover the different environments considered for the next generation cellular systems. For beyond-3G, we propose prefiltering for indoor and pedestrian microcell environments, beamforming for suburban macrocells including high-speed train, and space-time coding for urban conditions with moderate to high speeds.**

Index Terms: **Antenna arrays, MIMO communication systems, mobile wireless systems, multi-carrier communication.**

I. INTRODUCTION

The recent third generation (3G) of mobile cellular systems aims at supporting various multimedia services from voice and low-rate to high-rate data with up to 144 kbps in vehicular, 384 kbps in outdoor-to-indoor, and 2 Mbps in indoor and picocell environments, in its current terrestrial version [1]. However, as the demand for wireless services increases, the physical layer must provide a flexible multiple-access with a higher capacity at low cost.

The success of mobile communications for the mass market in the future will depend on the availability of attractive applications for end users. In order to meet the quality of service requirements of new multimedia applications, the next generation systems must be able to offer data-rates significantly greater than 2 Mbps. The European vision for a beyond-3G (also called 4G) system is a short-packet-based integrated system offering a wide range of services in all environments, and supporting various terminal classes. A set of target data-rates for end users can be defined depending on the environment: More than 100 Mbps in indoor and picocell under 10 km/h, 20–50 Mbps up to 60 km/h in urban environments, and 10–20 Mbps at 300 km/h (including train), using a 50 MHz bandwidth [2], [3]. Evidently, these requirements cannot be addressed with current UMTS standards.

Multi-carrier code division multiple-access (MC-CDMA) is one of the most promising multiple-access scheme for achieving such high data-rates, specially for the downlink (DL), i.e., from base station (BS) to mobile terminal (MT) [4]. This technique combines efficiently an orthogonal frequency division multiplex (OFDM) and code division multiple-access (CDMA). Therefore, MC-CDMA benefits from OFDM characteristics such as high spectral efficiency and robustness against multipath propagation, and CDMA advantages like flexibility and good interference properties for cellular environments [5]. However, MC-CDMA like all CDMA-based systems is limited by the multiple-access interference (MAI) induced by the loss of orthogonality among the users after multipath propagation. In conventional MC-CDMA downlink, the MAI is mitigated by frequency domain equalization techniques at MT. Since low complexity is required at MTs, we mainly consider simple single-user detection (SUD) techniques for implementation [6], [7], limiting the MAI cancellation capability.

Recent studies have shown that multiple-input multiple-output (MIMO) systems, using antenna arrays at both sides (BS and MT), yield substantial increases in channel capacity compared to single-input single-output (MISO) systems [8]–[10]. These capacity enhancements are based on the premise that a rich scattering environment provides independent transmission paths from each transmit (TX) antenna to each receive (RX) antenna. It has been shown [11], [12] that the combination of antenna arrays with MC-CDMA systems is very advantageous in mobile communications, even in multiple-input single-output (MISO) cases. At the European level, the combination of MIMO techniques with MC-CDMA has been studied during three years within the IST FP5 project MATRICE [2]. The European IST FP6 project 4MORE [3] aims at enhancing MATRICE by advancing one step towards an optimized implementation. In this project, performance degradation due to additional imperfections, like radio-frequency impairments, is studied as well. This paper intends to present the different MISO/MIMO approaches

Manuscript received February 15, 2005.

F. Portier, J-Y. Baudais, and J-F. Hélard are with the Institute of Electronics and Telecommunications in Rennes, France, email: {fabrice.portier, jean-yves.baudais, jean-francois.helard}@insa-rennes.fr.

I. Raos and S. Zazo are with the E.T.S.I. Telecomunicación, Universidad Politécnica de Madrid, Spain, email: {ivana, santiago}@gaps.ssr.upm.es.

A. Silva and A. Gameiro are with the Dept. Elect. & Telec., Inst. Telec, Univ. Aveiro, Portugal, email: asilva@av.it.pt, amg@det.ua.pt.

that have been studied for the downlink within the MATRICE project, and to propose solutions in order to cover the different environments considered for the next generation mobile communications. These techniques can be classified according to the degree of channel state information (CSI) available at transmitter:

- Complete CSI, for which space-time/frequency prefiltering strategies are optimal [13]. If BS has instantaneous CSI, the best solution is to adapt the transmitted signal to the channel fading. Considering time division duplex (TDD), prefiltering at transmitter side is performed using the inherent channel reciprocity between the uplink and downlink transmission periods. The CSI estimation from uplink can be used to improve the performance in downlink by reducing the MAI term at the mobile terminal or improving the signal to interference plus noise ratio (SINR). However, these techniques are reliable only for indoor or pedestrian environments, i.e., for low mobility scenarios. The aim of these algorithms is to allow the use of simple low-cost, low-consuming MT, while providing a performance usually superior to the one that would be obtained with multi-user detection (MUD). Transmit space-frequency prefiltering applied to MC-CDMA is a subject that came up only recently [14], [15].
- Partial CSI, for which sub-optimal prefiltering and beamforming algorithms can be studied. We generally have information about spatial parameters that are not as variable as channel frequency response, like spatial autocorrelation matrix or angle of arrival (AoA) of main paths. Those estimates can be used to perform transmit beamforming, that is principally suitable when the spatial correlation between TX-antennas and the spatial separation between users are significant. Algorithms considered assume partial CSI, more precisely an averaged spatial autocorrelation matrix. Averaging is done in frequency domain considering perfect CSI available on one subset of the total available subcarriers at BS. Therefore, frequency-invariant beamforming weights are calculated, over the whole bandwidth, to improve signal to noise ratio (SNR) or to point to the main (AoA) of the considered user. This approach combined with MC-CDMA was published in [16] and [17].
- Unavailable CSI, for which space-time codes (STC) have been proposed. In contrast to the previous approaches that try to exploit the fading over the MIMO channel, the goal is to mitigate fading effect, avoiding deep fades by averaging symbol information over multiple paths gains. STC spread information across antennas and time to benefit from transmit diversity. The first STC scheme was proposed by Alamouti [18] for two TX-antennas and one RX-antenna, and Tarokh [19] generalized orthogonal coding to a higher number of TX-antennas. These space-time block codes (STBC) based on an orthogonal transmission matrix provide full spatial diversity gains, no inter-symbol interference (ISI), and low-complexity maximum-likelihood receivers over frequency non-selective channels. Moreover, with orthogonal STBC, a single-antenna receiver can be used; in such a MISO design with two TX- and one RX-antennas, Alamouti STBC is also optimal from a capacity point of view, when no CSI is available at transmitter. The main advantages of the combination of STBC with MC-CDMA were detailed in [20] and [21].

This paper presents three downlink MIMO MC-CDMA schemes, one from each of the categories listed above: Transmit space-frequency prefiltering based on constrained zero-forcing (CZF) algorithm with complete CSI, transmit beamforming based on averaged SNR maximization (MSNR) or AoA with partial CSI, and orthogonal STBC based on Alamouti scheme without CSI at transmitter. We also compare these algorithms for different scenarios with perfect and imperfect channel estimates. As our system approach is valid only considering a global layer-1 process, we take into account the channel coding to treat the remaining diversity over each transmitted packet, using turbo-coding (TC). We then introduce average performance for the physical layer without considering upper-layer processing or optimizations that could adapt transmission flow to the channel state, especially for non-real-time traffic.

The paper is organized as follows. Section II describes the general downlink MIMO MC-CDMA system. In Section III, the three proposed transmit schemes are developed, according to the degree of CSI available at transmitter. Section IV presents the 3GGP-like MIMO channel model and the simulations parameters. Section V provides simulation results for the three considered algorithms, in a common urban scenario. Section VI discusses the validity of previous results and gives inputs concerning the variation of performance in other scenarios, in order to propose a strategy to fill beyond-3G requirements. Finally, the main conclusions are pointed out in Section VII.

In this paper, we will use the following notations. Bold upper letters denote matrices, and bold lower letters stand for column vectors, unless stated. $\boldsymbol{I}_N$ denotes the identity matrix of size $(N \times N)$; $\mathrm{diag}\{a_1 \cdots a_N\}$ denotes a $(N \times N)$ diagonal matrix with diagonal entries $a_1 \cdots a_N$. $E[\alpha]$ denotes the expected value of α; $\otimes$ is the Kronecker product. For matrix manipulations, we will use the following superscripts: $[\cdot]^{\mathsf{T}}$ denotes matrix transposition, $[\cdot]^*$ denotes complex conjugate, and their combination for matrix Hermitian is noted $[\cdot]^{\mathsf{H}}$.

II. GENERIC TRANSMISSION SCHEME

A. Downlink MC-CDMA Design

The studied MC-CDMA system and radio context are defined as follows. It combines a multiple-access through Walsh-Hadamard spreading sequences of length S_f, and a multicarrier modulation through classical (non-oversampled rectangular shape in time) OFDM with guard-interval Δ. N_c of the N_{fft} subcarriers are used for data. For each subcarrier p, the channel response $h^p(t)$ varies in time depending on mobility, and adjacent subcarriers are correlated in the frequency domain depending on multipath propagation. These channel properties are taken into account in the design of presented algorithms to benefit from the channel correlation or diversity.

From these inputs, we have options to optimize the discrete-time baseband equivalent model. The guard-interval duration is chosen larger than the delay spread of the impulse response to avoid ISI. Moreover, using a cyclic-prefix (CP) for guard-interval will reduce the constraint of precise FFT window, and

avoid inter-carrier interference (ICI) since we assume perfect synchronization. For bandwidth efficiency and to obtain flat-fading per subcarrier in an outdoor context, the OFDM-symbol duration T_x is increased by increasing N_{fft}. Then, for a given OFDM-symbol, the channel can be represented in the frequency domain by a single coefficient on each subcarrier. However, OFDM-symbol duration (and then the number of subcarriers) must be restrained for complexity issues and to ensure a low channel variation in time over OFDM-symbols, in order to perform a correct decoding. In particular, for Alamouti STBC applied in time, the decoding algorithm assumes channel invariance over two OFDM-symbols. The consequent parameter choices are given in Section IV. With N_c multiple of S_f, several solutions of chip-mapping are available [21]. In this paper, we present results with 1D-spreading in frequency, using a linear frequency interleaving, in order to allow each spread-symbol to benefit from the frequency diversity offered by the whole bandwidth.

Nevertheless, channel impairments introduce several limits for the system. Frequency diversity is welcome in a single-user case, but can eliminate the CDMA orthogonality between users. Moreover, additive white Gaussian noise (AWGN) corrupts the received signal. To finely overcome these two effects, we need to know the channel at transmitter or at receiver, performing pre- or post-equalization. In downlink, the broadcasted signal allows simple equalizations at MT, estimating the channel from known pilot-symbols for example, while in uplink, as each user's signal experiences a different channel, BS generally does not have information of all users' channels over all the bandwidth. That is why we often assume complete CSI at MT, while CSI at BS is limited and suboptimal algorithms need to be implemented.

B. Spatial Dimension Benefits

Multiple antennas at transmitter and at receiver offer a new dimension to the previous system, allowing a capacity gain depending on the channel matrix properties. We will consider a realistic system with a maximum of $M = 4$ TX-antennas, and up to $N = 2$ RX-antennas, since the BS usually provides more space flexibility. For each subcarrier, we will now consider a channel matrix $\boldsymbol{H}^p(t)$ of size $(N \times M)$, whose entries can be statistically correlated.

In this paper, we present MIMO schemes with a rate of 1, i.e., the additional space-time-frequency processing does not change the data-rate, but is used to increase the SINR for a given user in prefiltering and beamforming strategies, or to increase the diversity by spreading data in space with STBC. This choice ensures a compatibility with single-antenna receivers. In particular, we only consider orthogonal STBC based on Alamouti scheme, as other orthogonal STBC have a lower rate suboptimal for capacity. Furthermore, non-orthogonal STBC with higher rates, like spatial multiplexing, imply more complex or ineffective receivers with a channel rank of 1, for instance with single-antenna receivers. We present STBC results with 2 TX-antennas and 1 or 2 RX-antennas. An extension to 4 TX-antennas for orthogonal STBC, like switched-Alamouti, would exhibit a negligible gain in performance. However, incrementing the number of RX-antennas, an additional gain is achieved and low-complexity processing is preserved.

Nevertheless, synchronization and channel estimation aspects are complicated when increasing the number of antennas at both sides. Concerning synchronization, the classical OFDM is well localized in time, but not in frequency, and the use of multiple antennas adds a spatial dimension. Concerning channel knowledge over frequency, time and space, estimation using low overhead leads to noisy coefficients. In this paper, we assume perfect synchronization and sampling, and give results with perfect and imperfect channel knowledge.

C. Common MIMO MC-CDMA Scheme

Fig. 1 shows a simplified MIMO MC-CDMA downlink system (framing processes are omitted), general enough to gather all schemes presented in this paper, with K active users transmitting streams over M antennas and received by user j over N antennas. After channel encoding and interleaving processes, bit streams are mapped to a constellation χ (QPSK or higher-order QAM). Each user k ($k = 1, \cdots, K$) provides $N_s = N_c/S_f$ symbols per OFDM-symbol t. These symbols $\boldsymbol{s}_k^t = \left[s_k^{t,1} \cdots s_k^{t,q} \cdots s_k^{t,N_s}\right]^{\mathsf{T}}$ are delivered to the main transmit block that depends on the chosen multi-antenna multi-user algorithm. If CSI is available at transmitter, the symbols are weighted in function of the user or subcarrier, while no CSI means that this space-time-frequency process is applied independently on the signals of all users, which are then spread and summed. Note that we can swap the linear space-time-frequency and spreading processes. For our three algorithms, the CDMA spreading is performed in the same way on each TX-antenna using orthogonal sequences $\boldsymbol{c}_k = \left[c_k^1 \cdots c_k^{S_f}\right]^{\mathsf{T}}$, where $\boldsymbol{c}_k$ is column k of the $(S_f \times K)$ Walsh-Hadamard matrix $\boldsymbol{C}$. The resulting multi-user chips $\boldsymbol{x}_m^t = \left[x_m^{t,1} \cdots x_m^{t,p} \cdots x_m^{t,N_c}\right]^{\mathsf{T}}$ are spanned over the M TX-antennas and N_c subcarriers after OFDM modulation. A chip-mapping process defines the positions of these chips over the bandwidth, performing a linear frequency interleaving in the presented results. OFDM modulation is a simple IFFT on $N_{fft} > N_c$ subcarriers to facilitate digital filtering using null subcarriers on edges of the band; it is followed by the insertion of a CP, creating a copy between the beginning and the end of the OFDM-symbol. The signals are transmitted over a channel

$$\boldsymbol{\mathcal{H}}^t = \left[\left(\boldsymbol{H}^{t,1}\right)^{\mathsf{T}} \cdots \left(\boldsymbol{H}^{t,p}\right)^{\mathsf{T}} \ldots \left(\boldsymbol{H}^{t,N_c}\right)^{\mathsf{T}}\right]^{\mathsf{T}},$$

with $\boldsymbol{H}^{t,p}$ of size $(N \times M)$, whose complex-Gaussian entries $h_{n,m}^{t,p}$ represent the channel response from antenna m to antenna n, on subcarrier p, at OFDM-symbol t. The channel is generated from a realistic 3GPP model, correlated in space, time and frequency, and assumed normalized. A white zero-mean complex-Gaussian noise $\boldsymbol{\nu}_n^t = \left[\nu_n^{t,1} \cdots \nu_n^{t,N_c}\right]^{\mathsf{T}}$ is added on each RX-antenna, where each noise term is independent. In other words, $E\left[\left|h_{n,m}^{t,p}\right|^2\right] = 1$ and $E\left[\left|\nu_n^{t,p}\right|^2\right] = N_0, \forall p, t, n$.

At the receiver, OFDM demodulation consists in a guard-interval removal and an FFT, assuming perfect synchronization. The vector obtained on antenna n in the frequency domain after OFDM demodulation and chip-demapping is $\boldsymbol{y}_n^t = \left[y_n^{t,1} \cdots y_n^{t,p} \cdots y_n^{t,N_C}\right]^{\mathsf{T}}$. The relation between this received

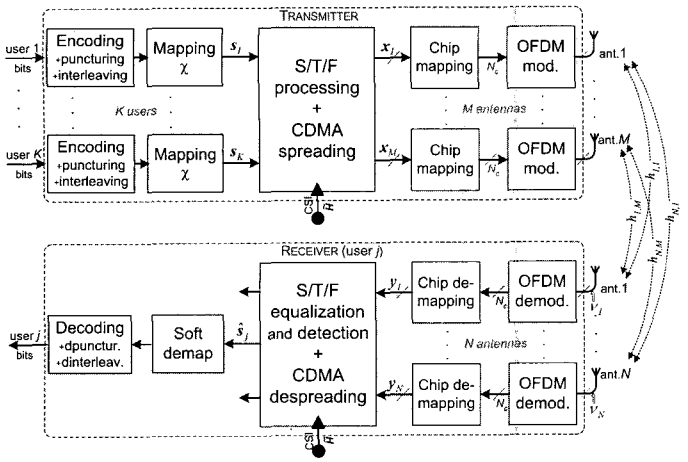

Fig. 1. Common MIMO MC-CDMA transmitter and receiver.

signal and the transmitted one is

$$\boldsymbol{y}_n^t = \boldsymbol{\mathcal{H}}_{(n)}^t \circ \boldsymbol{\mathcal{X}}^t + \boldsymbol{\nu}_n^t, \tag{1}$$

where $\circ$ is element-wise product between $(N_c \times M)$ matrices $\boldsymbol{\mathcal{H}}_{(n)}^t$ and $\boldsymbol{\mathcal{X}}^t = [\boldsymbol{x}_1^t \cdots \boldsymbol{x}_M^t]$. $\boldsymbol{\mathcal{H}}_{(n)}^t$ is an excerpt of $\boldsymbol{\mathcal{H}}^t$ concerning RX-antenna n.

If several RX-antennas are considered, equalization takes into account the frequency and spatial dimensions. If STBC is applied in time, several OFDM-symbols are considered for detection. After that, as we only consider single-user detection in our algorithms for complexity issues, user j is easily extracted from the multi-user signal by multiplication with its spreading code $\boldsymbol{c}_j$. Detected symbols $\hat{\boldsymbol{s}}_j^t = \left[\hat{s}_j^{t,1} \cdots \hat{s}_j^{t,p} \cdots \hat{s}_j^{t,N_s}\right]^{\mathsf{T}}$ are soft estimations of the symbols $\boldsymbol{s}_j^t$. A soft demapping is followed by decoding processes to deliver the bit stream of user j.

Concerning CSI at transmitter and receiver, we will consider perfect channel knowledge, or imperfect knowledge with matrices $\tilde{\boldsymbol{H}}^{t,p}$. These matrices are generated from the perfect ones, adding a white complex-Gaussian noise on each entry $h_{n,m}^{t,p}$, with a variance defined in Section IV.

III. MULTI-ANTENNA PROCESSING

From a common MC-CDMA system, performance improvement implies to take benefit from channel properties and variations in frequency/time/space, increasing SNR at receiver side for a given user, decreasing MAI, and avoiding deep fades. Antenna processing and equalization try to meet these requests, and this section presents three typical algorithms, as mentioned above.

A. Transmit Space-Frequency Prefiltering Based on CZF Algorithm with Complete CSI

In this subsection, we develop a space-frequency prefiltering algorithm that has two main advantages: Reducing the MAI at MTs by pre-formatting the signal so that the received signal at decision point is free from interferences, and allowing a transfer of computational burden from MT to BS. Using an antenna array at BS, the prefiltering can be done in space and frequency dimensions. We propose to jointly optimize the user separation in space and frequency by the use of criteria based on the decision variable after despreading at MT. This technique requires complete CSI at transmitter, and then, is suitable for systems with channel reciprocity between UL and DL, like TDD systems with low mobility. Concerning the receiver, we propose a single-antenna system with an OFDM demodulation, chip-demapping and despreading operations, i.e., we do not perform channel equalization, keeping the MT at low complexity.

In the prefiltering case, the $S_f M$ chips for user k and symbol $q = [1, \cdots, N_s]$ are weighted by a column vector $\boldsymbol{w}_k^q = \left[\boldsymbol{w}_{k,1}^{q\,\mathsf{T}} \cdots \boldsymbol{w}_{k,M}^{q\,\mathsf{T}}\right]^{\mathsf{T}}$ where $\boldsymbol{w}_{k,m}^q$ contains the S_f coefficients that weights the chips for antenna m. These weights are calculated using the CSI according to the criterion presented below. The decision variable at MT j is

$$\hat{s}_j^q = \underbrace{\boldsymbol{c}_j^{\mathsf{H}} \sum_{m=1}^{M} \left(\boldsymbol{h}_{j,m}^q \circ \boldsymbol{w}_{j,m}^q\right) \circ \boldsymbol{c}_j s_j^q}_{\text{Desired signal}} + \underbrace{\boldsymbol{c}_j^{\mathsf{H}} \sum_{i=1, i\neq j}^{K} \sum_{m=1}^{M} \left(\boldsymbol{h}_{j,m}^q \circ \boldsymbol{w}_{i,m}^q\right) \circ \mathbf{c}_i s_i^q}_{MAI} + \underbrace{\mathbf{c}_j^{\mathsf{H}} \boldsymbol{\nu}_j}_{\text{Noise}}, \tag{2}$$

where $\boldsymbol{h}_{j,m}^q$ is the channel frequency response vector of size S_f for user j, data symbol q, and antenna m, and $\boldsymbol{\nu}_j$ contains the noise samples on the S_f subcarriers. The signal of (2) involves three terms: The desired signal, the MAI caused by the loss of code orthogonality among the users, and the residual noise after despreading.

The prefiltering algorithm is based on a zero-forcing criterion, since we constrain the MAI term to be null, at all mobile terminals at the same time. Furthermore, as it takes into account the transmit power at BS, we call it the constrained zero-forcing algorithm. Applying the zero-forcing criterion to (2), we ensure that each user receives a signal that is free from MAI after despreading. The first term on the right side of (2), which is the desired signal, is strained to a constant for normalization purposes, while the second term, which represents the interference caused by other $(K-1)$ users, should be equal to zero.

The interference that the signal of user k produces at another MT j is obtained for a generic data symbol according to (2),

$$MAI(k \rightarrow j) = \boldsymbol{c}_j^{\mathsf{H}} \sum_{m=1}^{M} \boldsymbol{h}_{j,m}^q \circ \boldsymbol{w}_{k,m}^q \circ \boldsymbol{c}_k = \boldsymbol{\varphi}_{j,k}^{\mathsf{T}} \boldsymbol{w}_k^q, \tag{3}$$

with $\boldsymbol{\varphi}_{j,k} = \hat{\mathbf{c}}_k \circ [\boldsymbol{h}_{j,1}^{q\,\mathsf{T}} \cdots \boldsymbol{h}_{j,M}^{q\,\mathsf{T}}]^{\mathsf{T}} \circ \hat{\mathbf{c}}_j^*$, and $\hat{\mathbf{c}}_k = [\mathbf{c}_k^{\mathsf{T}} \cdots \mathbf{c}_k^{\mathsf{T}}]^{\mathsf{T}}$ is a column vector of size MS_f since the same code is used for all antenna branches.

The weight vector for user j is then obtained by constraining the desired signal part of its own decision variable to a constant ξ_j^q while canceling its MAI contribution at all other mobile terminals at the same time. This leads to the following set of conditions:

$$\begin{cases} \boldsymbol{c}_j^{\mathsf{H}} \left(\sum_{m=1}^{M} \boldsymbol{h}_{j,m}^q \circ \boldsymbol{w}_{j,m}^q \circ \boldsymbol{c}_j\right) = \xi_j^q \\ \boldsymbol{c}_k^{\mathsf{H}} \left(\sum_{m=1}^{M} \boldsymbol{h}_{k,m}^q \circ \boldsymbol{w}_{j,m}^q \circ \boldsymbol{c}_j\right) = 0, \forall k \neq j. \end{cases} \tag{4}$$

Therefore, to compute the weights for user j, we have to solve a linear system of K equations (constraints) and $S_f M$ variables (degrees of freedom), where $\mathbf{A}_j^q$ is a matrix of size $(K \times MS_f)$ given by $\boldsymbol{A}_j^q \boldsymbol{w}_j^q = \boldsymbol{b}$

$$\boldsymbol{A}_j^q = \begin{bmatrix} \left[\boldsymbol{h}_{j,1}^q{}^{\mathsf{T}} \cdots \boldsymbol{h}_{j,M}^q{}^{\mathsf{T}}\right] \\ \boldsymbol{\varphi}_{0,j}^{\mathsf{T}} \\ \vdots \\ \boldsymbol{\varphi}_{j-1,j}^{\mathsf{T}} \\ \boldsymbol{\varphi}_{j+1,j}^{\mathsf{T}} \\ \vdots \\ \boldsymbol{\varphi}_{K-1,j}^{\mathsf{T}} \end{bmatrix}, \quad \boldsymbol{b} = \begin{bmatrix} \xi_j^q \\ 0 \\ \vdots \\ 0 \end{bmatrix}. \tag{5}$$

The prefiltering algorithms should take into account the minimization of the transmit power. Therefore, the transmit power must be minimized under the K above constraints. When the number of constraints equals the number of degrees of freedom, a single solution exists if there are no singularities. However, if we have more degrees of freedom than constraints $(S_f M > K)$ then signal can be designed to optimize a cost function, like the total transmit power. The higher $(S_f M - K)$ is, the more effective optimization will be. This optimization can be solved with the Lagrange multipliers method. After mathematical manipulations [12], we obtain the CZF based prefiltering vector,

$$\boldsymbol{w}_j^q = \zeta_j^q \boldsymbol{A}_j^{q\mathsf{H}} (\boldsymbol{A}_j^q \boldsymbol{A}_j^{q\mathsf{H}})^{-1} \boldsymbol{b} = \zeta_j^q \boldsymbol{A}_j^{q\mathsf{H}} \boldsymbol{\Psi}_j^q \mathrm{b}, \tag{6}$$

where $\boldsymbol{\Psi}_j^q = (\boldsymbol{A}_j^q \boldsymbol{A}_j^{q\mathsf{H}})^{-1}$ is a square and Hermitian matrix of size $(K \times K)$, and ζ_j^q is a constant used to normalize the vector weight according to $|\boldsymbol{w}_k^q|^2 = \boldsymbol{w}_k^{q\mathsf{H}} \boldsymbol{w}_k^q = 1, \forall k = 1, \cdots, K$.

Last equation shows that the most computational intensive task, to calculate the weights, is matrix $\boldsymbol{\Psi}_j^q$ inversion. However, the size of this matrix is just $(K \times K)$, independently of the spreading factor and the number of antennas, which makes this algorithm very attractive for practical implementations.

B. Transmit Beamforming Based on Spatial Correlation Matrix with Partial CSI

Transmit beamforming is a purely-spatial prefiltering technique that allows spatially-selective transmissions based on instantaneous or long-term channel knowledge at BS. The second approach is useful in rapidly variable channels where averaged spatial information is not as variable as instantaneous CSI, and then, can be applied in TDD scenarios with mobility and in FDD schemes, where instantaneous channel knowledge is unavailable at the transmitter. Moreover, the considered signal bandwidth is very large and channel exhibits frequency selectivity. Thus, what can be considered "constant" is spatial information like AoA or spatial autocorrelation matrix.

Considering transmit beamforming with wideband MC-CDMA, we must notice two limits. First, each user, independently of others, has its specific beamforming weights, which is equivalent to experience different propagation channels; this fact may require more complex processing at receiver if MAI has to be minimized, like in uplink MC-CDMA. Secondly, one of the best known beamforming method in multi-user systems is pointing to the most significant AoA, and putting nulls in AoA of other users; however, this strategy is not adequate for our wideband scenario in which energy arrives from a very wide angle spread.

Then, the schemes analyzed assume beamforming weights that are frequency-invariant over the whole bandwidth, and either maximize user average SNR or point to the main AoA.

B.1 Single-User Solution

Assuming a single-user case, optimum solution in terms of SNR maximization is well known. We define $\mathbf{H}$ the MISO channel matrix $(S_f \times M)$ from BS to this user and $\mathbf{V}$ the beamforming set of vectors sized $(S_f M \times 1)$:

$$\begin{aligned} \mathbf{H} &= [(\boldsymbol{h}^1)^{\mathsf{T}} \cdots (\boldsymbol{h}^{S_f})^{\mathsf{T}}]^{\mathsf{T}} \\ \mathbf{V} &= [(\boldsymbol{v}^1)^{\mathsf{T}} \cdots (\boldsymbol{v}^{S_f})^{\mathsf{T}}]^{\mathsf{T}}, \end{aligned} \tag{7}$$

where $\boldsymbol{h}^p$ stands for the corresponding row vector of matrix $\mathbf{H}$ associated to frequency p.

Received vector on S_f subcarriers (corresponding to one MC-CDMA symbol) after OFDM demodulation and chip-demapping can be described in the frequency domain by (8) where $\mathbf{C} = \mathrm{diag}\{\boldsymbol{c}\}$ is a diagonal matrix with user code $\boldsymbol{c}$ on the main diagonal, s is the transmitted symbol and $\boldsymbol{\nu}$ are AWGN samples.

$$\boldsymbol{y} = \mathbf{C}\mathrm{diag}\left\{\boldsymbol{h}^1 \cdots \boldsymbol{h}^{\mathrm{S_f}}\right\} \mathbf{V}\mathrm{s} + \boldsymbol{\nu}. \tag{8}$$

Optimum solution presented in (9) is based on the maximum ratio combining concept where $\|\cdot\|_F$ is Frobenius norm, and $\boldsymbol{v}^p$ are the Hermitian normalized rows of matrix $\boldsymbol{h}^p$.

$$\boldsymbol{v}^p = \frac{(\boldsymbol{h}^p)^{\mathsf{H}}}{\|\boldsymbol{h}^p\|_F}, 1 \le p \le S_f. \tag{9}$$

This approach has been described in [11]. However, as it requires complete CSI, we will not develop it in this contribution. Indeed, perfect CSI is available in TDD modes if both links use the same sets of carriers per user, but this hypothesis is unrealistic in FDD (without feedback) or even TDD where channel reciprocity is not applicable. This case arises if another multiple-access scheme is used in UL, e.g., SS-MC-MA [22] where different users are frequency multiplexed over different sets of carriers to simplify uplink synchronizations and channel estimation.

B.2 Averaged MSNR Algorithm

Here, we present an alternative to the simpler phased array proposal, based on the estimation of the spatial autocorrelation matrix. The new signal model considering a common beamformer for all the carriers can be stated as follows:

$$\boldsymbol{y} = \mathbf{C}\mathbf{H}\boldsymbol{w}s + \boldsymbol{\nu}, \tag{10}$$

where $\boldsymbol{w}$ is a $(M \times 1)$ vector. Standard SNR maximization problem can be formulated as a Rayleigh quotient

$$\boldsymbol{w}^p = \max_{\boldsymbol{w}^i} \frac{\boldsymbol{w}^{i\mathsf{H}} \boldsymbol{h}^{p\mathsf{H}} \boldsymbol{h}^p \boldsymbol{w}^i}{\boldsymbol{w}^{i\mathsf{H}} \boldsymbol{w}^i}, \tag{11}$$

where the optimum solution is the eigenvector of $\boldsymbol{R}^p = \boldsymbol{h}^{p\mathsf{H}}\boldsymbol{h}^p$ corresponding to the maximum eigenvalue. $\boldsymbol{R}^p$ is the specific spatial autocorrelation matrix for this channel trial and, being channel dependent, can not be used in the partial CSI case. However, instead of the instantaneous matrix $\boldsymbol{R}^p$, an averaged estimation of this matrix can be implemented,

$$\boldsymbol{w} = \max_{\boldsymbol{w}_i} \frac{\boldsymbol{w}_i^{\mathsf{H}} E[\boldsymbol{h}^{p\mathsf{H}}\boldsymbol{h}^p]\boldsymbol{w}_i}{\boldsymbol{w}_i^{\mathsf{H}}\boldsymbol{w}_i}, \tag{12}$$

where matrix $\hat{\boldsymbol{R}} = E[\boldsymbol{h}^{p\mathsf{H}}\boldsymbol{h}^p]$ can be estimated by frequency averaging in the uplink and used to design the suboptimum beamformer in downlink. This frequency domain averaging is performed over calculated autocorrelation matrices from channel frequency response estimates over all subcarriers dedicated to the desired user. Users beamformer weights $\boldsymbol{w}_k$ are given by the eigenvector associated with the maximum eigenvalue obtained from eigendecomposition of this averaged autocorrelation matrix. As this beamforming scheme is frequency-invariant but user specific, it must be performed before summing of spreaded users' chips in transmitter. After performing beamforming weighting, user symbols are adequately grouped and fast Hadamard transform (FHT) spreading is performed on each TX-antenna.

B.3 Averaged AoA Algorithm

Another possibility to benefit from available spatial information is to extract main AoA from estimated spatial autocorrelation matrix. The applied algorithm for its estimation is the Bartlett one, as it has low complexity and is found to have sufficiently good performance, even compared with Capon estimation [23]. Bartlett estimation consists in maximization of the following spatial spectrum expression:

$$\theta = \max_{\theta_i} \mathbf{a}(\theta_i)^{\mathsf{H}} E\left[\mathbf{H}^{\mathsf{H}}\mathbf{H}\right] \mathbf{a}(\theta_i), \tag{13}$$

where $\mathbf{a}(\theta_i)$ is steering vector pointing to angle θ_i. This algorithm is simpler than averaged MSNR; however, when a small number of TX-antennas is available at transmitter, their beamwidth does not allow very accurate adaptation to the receive energy diagram. In this case, the beamforming weight per TX-antenna m ($m = 0, \cdots, M-1$) is

$$\boldsymbol{w}_m = e^{jm\frac{2\pi d}{\lambda}\sin\theta}. \tag{14}$$

B.4 Receiver Processing

At receiver, conventional single-RX-antenna MC-CDMA signal processing is performed as users are not aware that beamforming is performed at BS. Therefore, after chip-demapping, the module called "S/T/F equalization and detection + CDMA despreading" in Fig. 1 performs minimum mean square error (MMSE) equalization per carrier, followed by Hadamard despreading. This way, the receiver remains simple, and the advanced signal processing is done at BS.

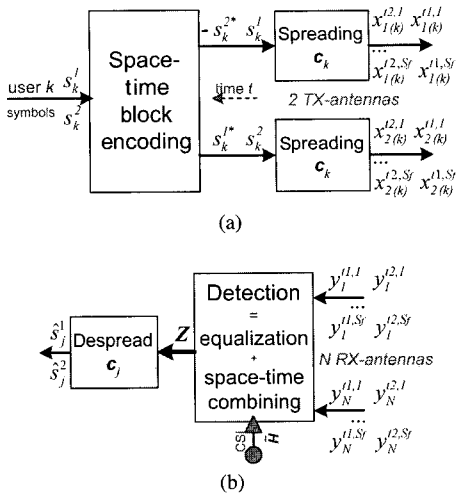

Fig. 2. STBC MC-CDMA details: (a) STBC and MC-CDMA spreading at transmitter for user k, (b) detection and despreading part at receiver of user j.

C. Orthogonal Space-Time Block Coding Algorithm without CSI at Transmitter

In this subsection, we describe orthogonal STBC based on Alamouti scheme with 2 TX-antennas, whatever the number of RX-antennas is. This scheme can be applied in all scenarios, although the presented decoding algorithm assumes channel invariance in time over two OFDM-symbols. The combination of STBC with MC-CDMA is simple since we apply the Alamouti coding over each subcarrier p of the system, as shown on Fig. 2. We present the STBC process before CDMA spreading at transmitter but we can swap these two linear processes. The coding is applied in time over two consecutive OFDM-symbols, assuming that channel variations in frequency are more important than in time in our scenario. This combination tries to benefit from the maximum diversity in space, time and frequency. After mapping, each user k simultaneously transmits two symbols $w_{k,1}^{t1} = s_k^1$ and $w_{k,2}^{t1} = s_k^2$ from both TX-antennas at time $t1$, then $w_{k,1}^{t2} = -\left(s_k^2\right)^*$ and $w_{k,2}^{t2} = \left(s_k^1\right)^*$ at time $t2 = t1 + T_x$. As this process is applied on each subcarrier, we drop the subcarrier index p. Dropping time index at the space-time encoder output, the data symbols of the K users $\boldsymbol{w}_1 = [w_{1,1} \cdots w_{k,1} \cdots w_{K,1}]^{\mathsf{T}}$ (the same for symbol $\boldsymbol{w}_2$) are multiplied by their specific orthogonal spreading code $\boldsymbol{c}_k$. FHT can be used in downlink to spread and sum data of all users, preserving their orthogonality until transmission. In the following equations, we consider only S_f subcarriers from 1D-spreading in frequency (classical MC-CDMA) without losing generality as the extension is straightforward. Each data symbol is then transmitted on S_f parallel subcarriers. The vector obtained at RX-antenna n after perfect OFDM demodulation and chip-demapping, at time $t1$ and $t2$, is given by

$$\boldsymbol{Y}_n = \boldsymbol{\mathcal{H}}_n \boldsymbol{\mathcal{C}} \boldsymbol{\mathcal{S}} + \boldsymbol{\Gamma}_n, \quad \boldsymbol{\mathcal{H}}_n = \begin{bmatrix} \boldsymbol{H}_{n,1} & \boldsymbol{H}_{n,2} \\ \boldsymbol{H}_{n,2}^* & -\boldsymbol{H}_{n,1}^* \end{bmatrix}, \tag{15}$$

where $\boldsymbol{Y}_n = \begin{bmatrix} \left(\boldsymbol{y}_n^{t1}\right)^{\mathsf{T}} & \left(\boldsymbol{y}_n^{t2}\right)^{\mathsf{H}} \end{bmatrix}^{\mathsf{T}}$ is a column vector of size $2S_f$, with $\boldsymbol{y}_n^t = \left[y_n^{t,1} \cdots y_n^{t,S_f}\right]^{\mathsf{T}}$;

where $\boldsymbol{H}_{n,m} = \text{diag}\left\{h^{1}_{n,m} \cdots h^{S_f}_{n,m}\right\}$;
where $\boldsymbol{\mathcal{C}} = \boldsymbol{I}_2 \otimes \boldsymbol{C}$;
where $\boldsymbol{\mathcal{S}} = \left[(\boldsymbol{s}^1)^{\mathsf{T}}(\boldsymbol{s}^2)^{\mathsf{T}}\right]^{\mathsf{T}}$ with $\boldsymbol{s}^q = [s^q_1 \cdots s^q_K]^{\mathsf{T}}$;
where $\boldsymbol{\Gamma}_n = \left[(\boldsymbol{\nu}^{t1}_n)^{\mathsf{T}}(\boldsymbol{\nu}^{t2}_n)^{\mathsf{H}}\right]^{\mathsf{T}}$ represents AWGN.

Channel invariance during two OFDM-symbols is assumed to permit the recombination of symbols, even if channel is slightly varying in high-speed scenarios. At the receiver, in order to detect the two transmitted symbols s^1_j and s^2_j for the desired user j, channel knowledge is necessary. It allows simple one-tap equalization per subcarrier, combined with a space-time block decoding. With such an orthogonal STBC, a simple linear decoding is performed as it provides results equivalent to an exhaustive maximum-likelihood research at low complexity. Thus, the two successive received MC-CDMA symbols are combined, equalized and added from the N RX-antennas to detect the two symbols. After despreading, the data symbols of user j are

$$\left[\hat{s}^1_j \hat{s}^2_j\right]^{\mathsf{T}} = \left(\boldsymbol{I}_2 \otimes \boldsymbol{c}^{\mathsf{T}}_j\right) \boldsymbol{Z} = \left(\boldsymbol{I}_2 \otimes \boldsymbol{c}^{\mathsf{T}}_j\right) \sum_{n=1}^{N} \boldsymbol{\mathcal{G}}_n \boldsymbol{Y}_n, \quad (16)$$

with

$$\boldsymbol{\mathcal{G}}_n = \begin{bmatrix} \boldsymbol{G}_{n,1} & \boldsymbol{G}^*_{n,2} \\ \boldsymbol{G}_{n,2} & -\boldsymbol{G}^*_{n,1} \end{bmatrix},$$

where $\boldsymbol{Z} = \left[z^1_1 \cdots z^1_{S_f} z^2_1 \cdots z^2_{S_f}\right]^{\mathsf{T}}$ is the vector of the received signals equalized and combined from the N antennas. $\boldsymbol{G}_{n,m}$ is a diagonal matrix, since we used an SUD scheme, containing the S_f equalization coefficients $g^p_{n,m}$ $(p = 1 \cdots S_f)$ for the channel between the TX-antenna m and the RX-antenna n. For instance, to detect s^1_i, the MMSE-SUD coefficients $g^p_{n,m}$ minimize the mean square value of error between the signal $\sum_{k=1}^{K} c^p_k s^1_k$ transmitted on subcarrier p and the signal z^1_p combined from the N RX-antennas by the Alamouti decoding. In the same way, the zero-forcing (ZF) coefficients $g^p_{n,m}$ restore the orthogonality between the different users. It is well known that with MISO systems, ZF leads to excessive noise amplification for low subcarrier SNR. In our MIMO case, spatial diversity, equal to the product $(N \times M)$ in the decorrelated situation, statistically reduces this occurrence. Thus, with an increasing number of antennas, ZF tends to MMSE efficiency, and does not require SNR estimation γ at receiver. We assume the same noise level statistically for each subcarrier or RX-antenna. Besides, knowledge of the spreading codes $\boldsymbol{c}_i$, $(i \neq j)$ of the interfering users is not required to derive the ZF and MMSE-SUD coefficients, as shown in the following MMSE equation:

$$g^p_{n,m} = \left(h^p_{n,m}\right)^* \Big/ \left[\sum_{m=1}^{2}\sum_{n=1}^{N} \left|h^p_{n,m}\right|^2 + \frac{1}{\gamma}\right]. \quad (17)$$

ZF equations are similar assuming $1/\gamma = 0$. Note that the threshold detection should be normalized by ρ for MMSE with high-order modulations. The sum is performed on the S_f subcarriers where the considered symbol is spread:

$$\rho = S_f \Big/ \sum_{p=1}^{S_f} \frac{\sum_{m=1}^{2}\sum_{n=1}^{N} \left|h^p_{n,m}\right|^2}{\sum_{m=1}^{2}\sum_{n=1}^{N} \left|h^p_{n,m}\right|^2 + \frac{1}{\gamma}}. \quad (18)$$

Table 1. Main MIMO channel parameters.

Channel profile	BRAN E
Maximum delay $\tau_{\max}$	1.76 μs
Number of paths	17
Number of sub-rays per path	20
Velocity	60 km/h in common scenario
Mean angle spread at BS	$E[\sigma_{AS}] = 21.4°$
Mean angle spread at MT	$E[\sigma_{AS,MT}] = 68°$
RMS delay spread	$E[\sigma_{DS}] = 0.25$ μs
Element spacing	0.5 λ – 10 λ

IV. CHANNEL MODEL AND SYSTEM PARAMETERS

A. MIMO Channel Model and Configuration

There are two main categories of MIMO channel models: First type contains directional information, whether geometrically or statistically based, second type is based on the statistical correlation. Models with directional information can be used both to evaluate beamforming and diversity techniques while the former one is not suitable for antenna use with directional techniques. As we are concerned with different usage of multiple antennas, the directional 3GPP-3GPP2 propagation model was simulated [24].

This MIMO spatial channel model is a hybrid approach between a geometrical concept depending on cluster positions and a tapped delay line model described by an average power delay profile with fixed number of taps. The difference of this model when compared to standardized tapped delay line model is the introduction of a variable θ for angular variations in azimuth-plane. Each scenario having its specific channel parameters, the IST-MATRICE project developed such a model with a set of scenarios adapted to the 5 GHz carrier frequency with 50 MHz bandwidth.

Table 1 summarizes the main MIMO channel parameters of our common urban propagation scenario, used to present results in Section V [25], [26]. It models the non-line-of-sight (non-LOS) BRAN E channel, characterized by a large delay spread and angular spread. Different users (channel realizations) are uniformly distributed within a 120 degrees sector, each one respecting the Table 1 parameters. Linear arrays are used at BS and MT, and simulations consider a TX-antenna spacing of 10 λ, and RX-antenna spacing of 0.5 λ, except for beamforming algorithms where TX-antennas are separated of 0.5 wavelengths. The consequent spatial correlation is inferior to 0.1 for an antenna spacing of 10 λ, while a 0.5 λ spacing leads to a correlation around 0.7 at BS, and 0.35 at MT. In the frequency domain, a measure of the coherence bandwidth is around 1.5 MHz. Correlation in time, derived from Doppler frequency, is given by the measured coherence time that is close to the frame duration at 60 km/h, where frame is defined as a packet of 30 OFDM-symbols.

B. System Parameters

The system parameters are chosen according to the time and frequency coherence of the channel in order to reduce ICI and ISI. Besides, investigated MC-CDMA configurations are designed to propose high throughput solutions for outdoor scenar-

Table 2. Main MIMO system parameters.

Sampling frequency F_s	57.6 MHz
FFT size N_{fft}	1024
Number of used subcarriers N_c	736
Guard interval duration Δ	3.75 μs
Total OFDM duration $T_x = T_u + \Delta$	21.52 μs
Subcarrier spacing $\Delta_f = 1/T_u$	56.2 kHz
Length S_f of spreading codes	32
Modulation (Gray mapping)	QPSK, 16QAM, 64QAM
Center frequency f_c	5.0 GHz
Occupied bandwidth B_f	41.46 MHz
Frame duration / guard duration	30 T_x / 20.8 μs

Table 3. Link between global-rate and data-rate.

R (bit/s/Hz)	1	2	3	4.5
class modul.	QPSK	16QAM	16QAM	64QAM
class coding	TC 1/2	TC 1/2	TC 3/4	TC 3/4
Data-rate (Mbit/s)	33.1	66.2	99.3	149

ios, as shown in Table 2.

The studied configuration is based on a sampling frequency multiple of the 3.84 MHz UMTS frequency, to obtain the same frame duration as UMTS (0.666 ms). So F_s is equal to $15 \times 3.84 = 57.6$ MHz. We consider a carrier frequency $f_c = 5$ GHz, an FFT size of 1024 with $N_c = 736$ used subcarriers. The guard-interval duration $\Delta = 3.75$ μs, chosen according to the maximum delay $\tau_{\max} = 3.5$ μs to avoid ISI, leads to a 18% spectral efficiency loss. An additional guard-interval is used between frames to allow TDD alternating DL and UL. The global spectral efficiency loss is then 20%, corresponding to a power efficiency loss of 0.97 dB. The overall data-rate is then 33.1 Msymbols/s, shared between users. The length S_f of the spreading codes is chosen to allow 32 users at full-load.

Interleaving and coding processes are applied over a whole frame of 30 OFDM-symbols, and taken from UMTS standards. In particular, the channel coding scheme is the turbo-code defined in current UMTS with a rate of $\frac{1}{3}$, using two 8-states parallel concatenated convolutional codes. This is combined with a puncturing process to have an overall coding-rate R_c of $\frac{1}{2}$ or $\frac{3}{4}$. Results are given for 6 iterations at the channel decoder.

We call global-rate R the theoretical spectral efficiency of the combination channel coding plus mapping plus multi-antenna coding. In other words, as we assumed a multi-antenna coding-rate equal to one, $R = \log_2|\chi| \times R_c$, where $|\chi|$ is cardinality of the mapping. Table 3 links maximal data-rates to R.

Results are presented assuming different degrees of channel estimation errors: Perfect CSI or imperfect CSI. In the imperfect case, we model these errors with a Gaussian noise; then, the "noise level" added on channel coefficients is proportional to the noise level in the channel, i.e., with variance that is α times the variance of the AWGN. In results, we call 'CHperfect' a perfect CSI, 'CHvar0.5' a CSI with $\alpha = 0.5$, and 'CHvar0.1' a CSI with $\alpha = 0.1$.

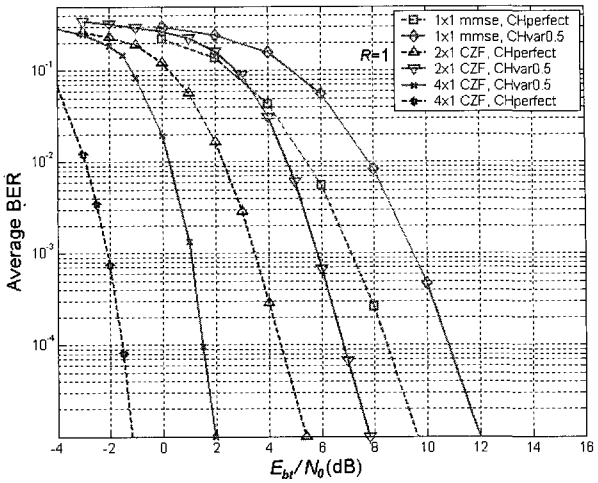

Fig. 3. Performance of MISO PF-CZF compared to SISO MMSE for QPSK TC$\frac{1}{2}$, full-load.

V. SIMULATION RESULTS

In this section, we present results obtained with three algorithms, in the common urban scenario defined in Section IV. Results are compared to MISO results with SUD based on the MMSE criterion, being the most efficient linear SUD scheme in full-load, but SISO ZF results are also presented. As reference, we also give MISO bounds in a Gaussian channel, i.e., an optimal channel flat in time and frequency only considering AWGN. In the three first subsections, performance is displayed as bit-error-rates (BER) versus E_{bt}/N_0, while the fourth subsection displays the corresponding data-rates computed from frame-error-rates (FER) versus E_{st}/N_0. E_{st}/N_0 represents the total transmit energy per symbol over the noise spectral density at each RX-antenna, and E_{bt}/N_0 represents the total transmit energy per useful bit over the noise spectral density at each RX-antenna. In the E_{bt}/N_0 value, we take into account the system parameters included in the global-rate R, but we do not consider the guard-interval efficiency loss and prospective framing overhead. Then, $(E_{st}/N_0) = R(E_{bt}/N_0)$. To compare algorithms with several antenna configurations, we assume a unitary total transmit power whatever the number of TX-antennas is. Thus, antenna gains are preserved; and in particular, MIMO results include the 3 dB gain when doubling the number of RX-antennas, due to independency between signal and noise. To limit the number of curves, we restrain presented results to full-load, unless stated.

A. Results with Transmit Space-Frequency Prefiltering

In this subsection, we present results for the CZF algorithm with perfect and imperfect CSI. Fig. 3 illustrates the performance of the CZF algorithm for 2 or 4 TX-antennas and 1 RX-antenna, with a global-rate of 1 bit/s/Hz considering QPSK modulation and half-rate turbo-coding. The CZF prefiltering outperforms the conventional SISO MMSE algorithm in all situations. When we increase the number of TX-antennas, thus enhance the separation in space, the performance of the CZF

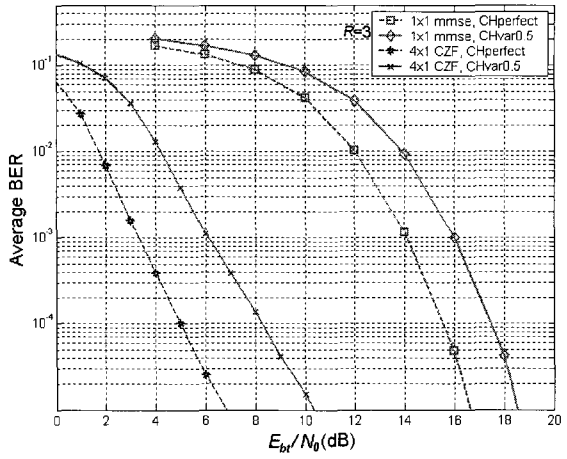

Fig. 4. Performance of MISO 4x1 PF-CZF compared to SISO MMSE for 16QAM TC$\frac{3}{4}$, full-load.

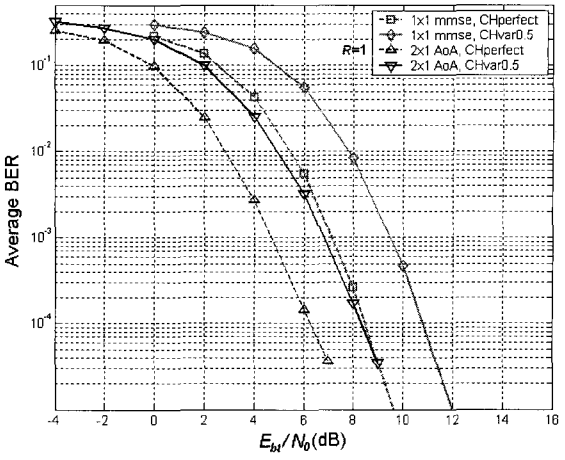

Fig. 6. Performance of MISO BF-AoA compared to SISO with MMSE equalization, QPSK TC$\frac{1}{2}$, full-load.

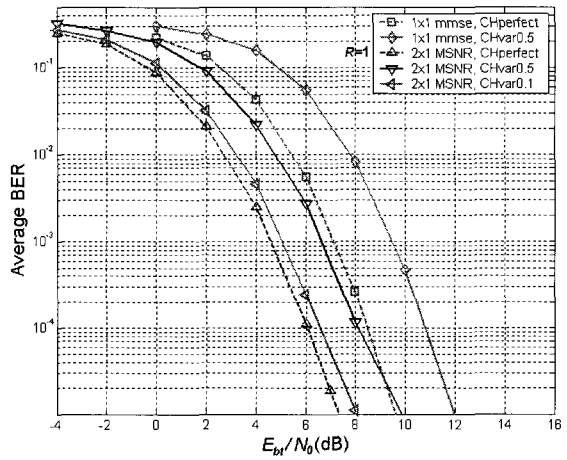

Fig. 5. Performance of MISO BF-MSNR compared to SISO with MMSE equalization, QPSK TC$\frac{1}{2}$, full-load.

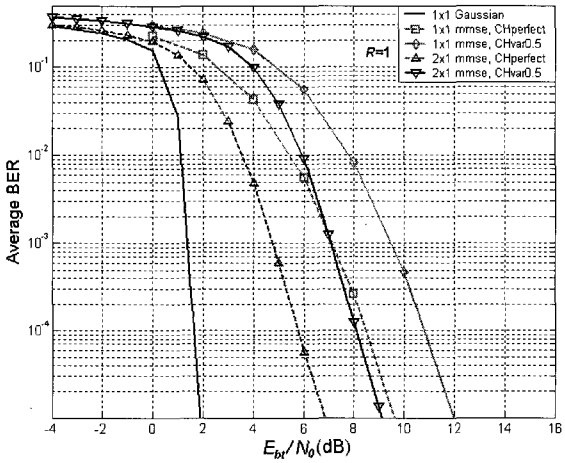

Fig. 7. Performance of MISO STBC compared to SISO with MMSE equalization, QPSK TC$\frac{1}{2}$, full-load.

improves. It should be noted that MMSE equalization implies estimations that increase the mobile complexity. Thus, the proposed algorithm outperforms SISO MMSE without involving an estimate of the channel or noise power at MT.

We also observe that the CZF algorithm is more sensitive to imperfect channel estimates when the number of antennas increases. With 2 and 4 TX-antennas, we obtain a penalty around 2 dB and 3 dB for BER=10^{-5}, respectively. However, the performance of the CZF with 4 TX-antennas and imperfect channel estimates is better than the one obtained with 2 TX-antennas and perfect estimates.

In order to assess the CZF algorithm in high throughput conditions, Fig. 4 presents results with a global-rate of 3 bit/s/Hz, considering 16QAM with a turbo-coding-rate $\frac{3}{4}$, and 4 TX-antennas. The same conclusion as for the previous figure can be pointed out. The penalty of imperfect channel estimates remains almost the same as in QPSK, i.e., we have a penalty around 3.2 dB for BER=10^{-5}.

B. Results with Transmit Beamforming

The performance of transmit beamforming algorithms with MMSE receiver for a global rate of 1 bit/s/Hz is given in Figs. 5 and 6, for MSNR and AoA algorithms, respectively, and compared to MISO references. Effect of imperfect CSI is shown for two values of error variance, considering it the same both at BS and MT. In BS, CSI errors influence the beamforming weights calculation, while in MT equalization errors appear. However, the imperfect CSI in MT is responsible for performance degradation while errors in BS lead to insignificant performance loss. The penalty for imperfect channel estimation (`CHvar0.5`) is 2 dB both for MSNR and AoA algorithms. The array gain causes better results with beamforming than MISO in the low SNR area of a Gaussian channel.

C. Results with Orthogonal Space-Time Block Coding

In this subsection, we present results with Alamouti space-time block coding, considering 2 TX-antennas and 1 or 2 RX-

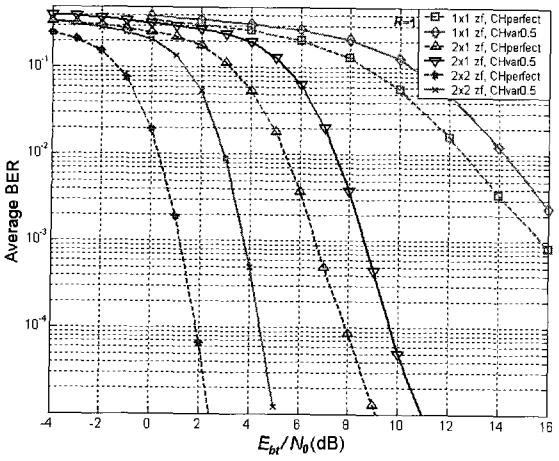

Fig. 8. Performance of SISO and MISO/MIMO STBC with ZF equalization, QPSK TC$\frac{1}{2}$, full-load.

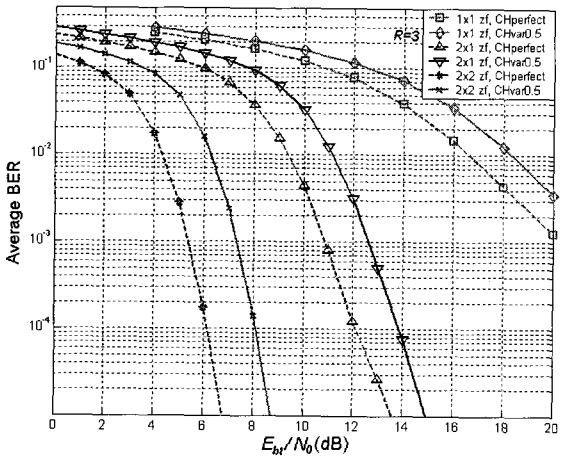

Fig. 9. Performance of SISO and MISO/MIMO STBC with ZF equalization, 16QAM TC$\frac{3}{4}$, full-load.

antennas. Two equalizations and two levels of CSI are considered at the receiver, and we present results for several global-rates. Figs. 7 and 8 present results with a global-rate of 1 bit/s/Hz, considering QPSK modulation with half-rate turbo-coding. The first one mainly illustrates performance of Alamouti STBC algorithm with 2 TX-antennas and 1 RX-antenna, MMSE equalization, and perfect or imperfect CSI. The MISO lower bound in a Gaussian channel is given as reference. We also give results in SISO MC-CDMA with MMSE equalization. Fig. 8 illustrates performance with ZF equalization, evaluating the gain between MISO, MISO, and MIMO configurations, with perfect or imperfect CSI.

Spatial diversity at transmitter allows performance to be closer to the Gaussian limit. The gain of MISO compared to MISO in this configuration is around 3 dB to obtain BER=10^{-5} with MMSE equalization. The degradation due to imperfect CSI is almost the same for MISO and MISO, around 2 dB whatever the equalization is. In all configurations, the degradation never exceeds 2.5 dB. MMSE gives better results than ZF but, when

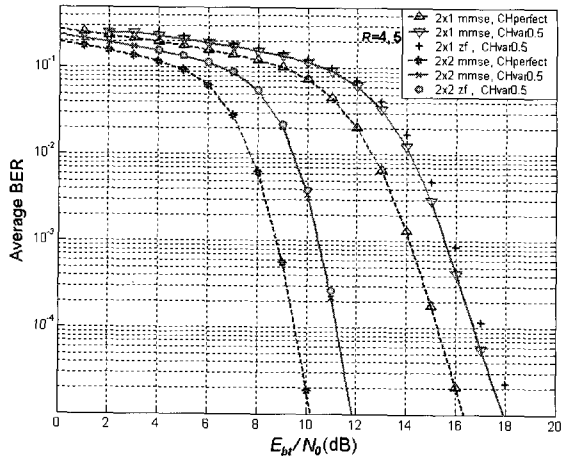

Fig. 10. Performance of MISO/MISO STBC with ZF/MMSE equalizations, 64QAM TC$\frac{3}{4}$, full-load.

increasing the number of antennas, the difference between these two equalization methods decreases. With 2 TX-antennas and 2 RX-antennas, the difference is around 0.5 dB in favor of MMSE to obtain BER=10^{-5}. However, ZF does not require SNR estimation at receiver.

Fig. 9 presents results with a global-rate of 3 bit/s/Hz, considering 16QAM with a turbo-coding-rate $\frac{3}{4}$. It illustrates performance with ZF equalization, evaluating the gain between MISO, MISO and MIMO configurations, with perfect or imperfect CSI. In this configuration with a high-order modulation, the gain of MIMO configurations over MISO ones increases again, and the difference between ZF and MMSE still decreases. With 2 TX-antennas and 2 RX-antennas, the difference is around 0.2 dB in favor of MMSE compared to ZF to obtain BER=10^{-5}.

Fig. 10 presents results with a global-rate of 4.5 bit/s/Hz, considering 64QAM with a turbo-coding-rate $\frac{3}{4}$. It illustrates performance of Alamouti STBC algorithm with 2 TX-antennas and 1 or 2 RX-antennas, with MMSE or ZF equalizations, and perfect or imperfect CSI. The trends observed in previous figures are confirmed. The gain of MISO and MIMO configurations over MISO ones has been shown, promising high data-rates with a simple equalization at receiver. In particular, performance with ZF equalization is almost the same as MMSE equalization in the 64QAM MISO and MIMO configurations considered. The degradation due to imperfect CSI is rather low, including when we consider high data-rates. In the 64QAM MISO and MIMO configurations considered, this degradation is less than 2 dB.

D. Conceivable Data-Rates

From the previous simulations, we present global data-rate results that the physical layer can reach, assuming the parameters defined in Section IV. This data-rate is calculated from correctly received frames, assuming a corresponding automatic-repeat-request process. As we need to put different global-rates on the same figure, we do not provide results versus E_{bt}/N_0, but versus E_{st}/N_0, assuming a normalized transmit signal E_{st}. The guard-interval efficiency loss is taken into account in the data-rate values, and thus, in the "Shannon's limit 33.1" presented in

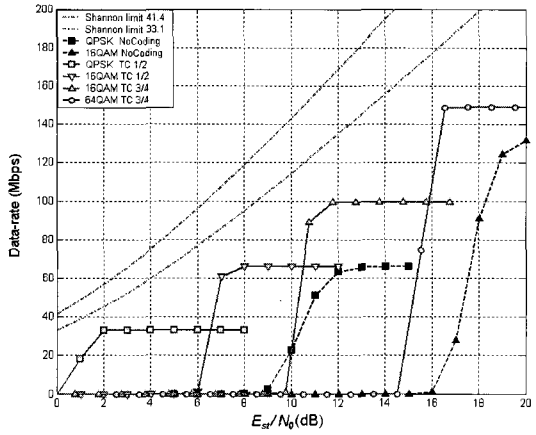

Fig. 11. Maximal data-rates with the considered SISO MC-CDMA system in Gaussian channel.

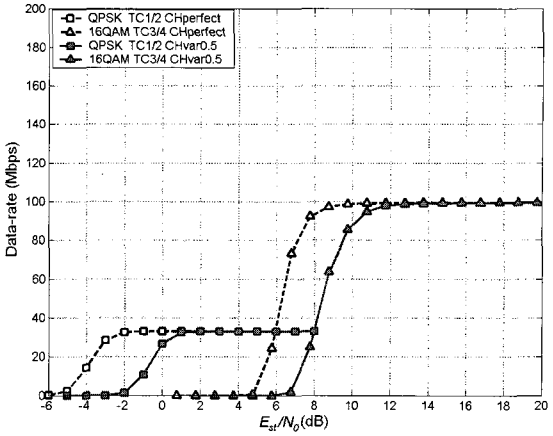

Fig. 13. Data-rates obtained with MISO 4×1 CZF prefiltering in the common scenario.

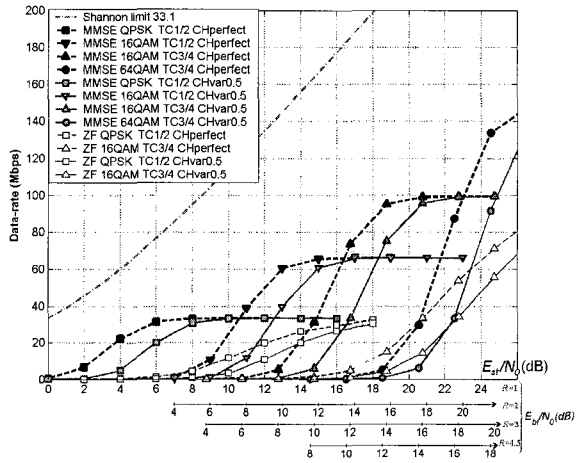

Fig. 12. Data-rates obtained with the considered SISO MC-CDMA system in the common scenario.

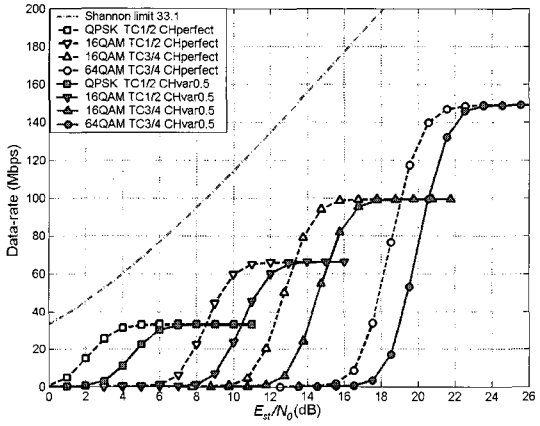

Fig. 14. Data-rates obtained with MISO 2×1 STBC and MMSE equalization in the common scenario.

Fig. 11. This upper bound corresponds to the MISO data-rate bound in a channel with an equivalent bandwidth of 33.1 MHz. This figure also presents the results in a Gaussian channel as the upper MISO bounds with the considered system including discrete modulations, with or without channel coding.

Fig. 12 shows the data-rates obtained with the considered SISO MC-CDMA system and MMSE equalization, in the common scenario, i.e., in a typical outdoor BRAN E channel. Perfect and imperfect CSI are considered, assuming that a real channel estimation algorithm would operate in the coloured areas between these references, depending on its quality. The SNR axis is E_{st}/N_0, but equivalent values of E_{bt}/N_0 for the considered global-rates are given.

Figures for the multi-antenna algorithms are then depicted in the common scenario. Fig. 13 shows the data-rates obtained with CZF transmit prefiltering, considering two classes of global-rates. Fig. 14 shows the data-rates obtained with Alamouti STBC, considering four classes of global-rates. It confirms the good results obtained in previous subsections and promise high throughput available for upper layers.

VI. STRATEGY IN A BEYOND-3G CONTEXT

This section discusses the limits of our model and the validity of previous results, and then gives inputs concerning the variation of performance in other scenarios, in order to propose a strategy to fill beyond-3G requirements.

A. Limits of Our Model and Validity of Previous Results

First, we did not consider intercell interference and thus, did not perform scrambling over the spreading process. However, in [27], Section 14 is dedicated to the analysis of intercell interference properties in SISO MC-CDMA and concludes that it can be modeled as AWGN. After that, this level of noise should depend on the spatial processes considered.

Secondly, the model used for channel estimation errors has limits, as we only considered complex-Gaussian noise on channel coefficients for imperfect CSI. However, the prefiltering and beamforming algorithms should also consider the delay impairment, in TDD, between channel estimation from UL and the use in DL. For beamforming that requires only a partial CSI, this delay and the errors at BS do not really affect performance. On the other side, prefiltering algorithms that require perfect CSI

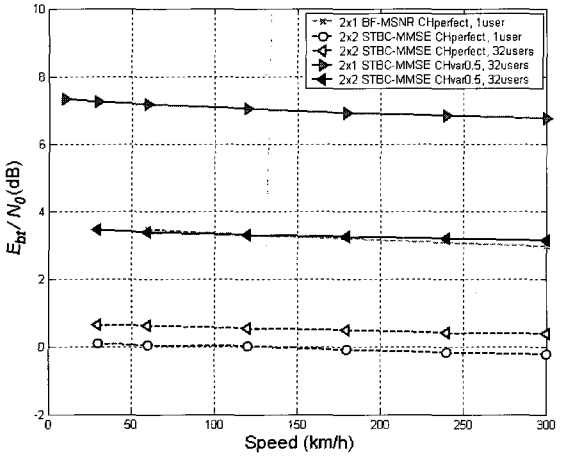

Fig. 15. Performance of algorithms depending on speed, QPSK TC$\frac{1}{2}$.

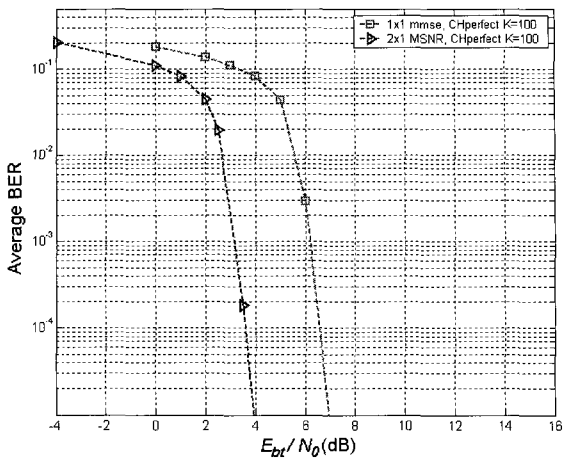

Fig. 16. Performance of MISO BF-MSNR depending on channel LOS for 16QAM TC$\frac{3}{4}$, full-load.

are the most optimistic cases. Then, such a CSI delay can be dramatic for CZF if it exceeds the coherence-time, and consequently limits the use of prefiltering to low-velocity scenarios.

Thirdly, the channel parameters used are typical of an outdoor scenario, but a full deployment requires a study over a wide range of scenarios. Beamforming processes are dependant of user's repartition and angle spreads, and the correlations in space, time, and frequency significantly influence performance of the three algorithms. Inputs are given, concerning speed and channel paths configuration, in the following subsection.

B. Expected Performance Depending on the Scenario

B.1 Effect of CSI Delays for Algorithms Requiring CSI at BS

Considering the CZF prefiltering algorithm, an outdated CSI introduces a significant degradation that limits this algorithm to low-speed scenarios, i.e., where the channel variation between the UL estimated frame and the considered DL frame is low.

Considering our transmit beamforming algorithms, CSI mismatches do not significantly influence beamforming weights calculation. The CSI delay at BS has a negligible effect, given that spatial information does not change substantially during one frame, even with high-speed MT. When comparing a scenario with perfect CSI available at each OFDM-symbol and a scenario with a constant CSI from the beginning of each frame, the degradation with a mobile speed of 120 km/h and a global rate of 1 bit/s/Hz is less than 0.1 dB.

B.2 Effect of Speed on Systems

Mobility has an effect on channel estimation and available CSI, but this has been partly studied in the previous parts and will not be considered here. The conclusion was that prefitering is not suitable in high-speed scenarios and transmit beamforming has shown its robustness to channel mismatches. Thus, here we focus on the effects that the channel variations have on the whole systems with a fixed CSI error (perfect CSI or `CHvar0.5`), to show the performance evolution of the decoding process in function of speed. Note that the channel estimation process may require more overhead when increasing speed, for this assumption to be valid. Fig. 15 shows the E_{bt}/N_0 required to obtain a FER of 10^{-2}, for beamforming or STBC. Beamforming algorithm is based on MSNR, without CSI errors, and STBC is tested with two antenna configurations, MMSE equalization, and `CHvar0.5`. Speed does not lead to significant variations of performance, but an improvement is observed when speed increases, as the additional diversity in time provided is used by the turbo-coding process over the frame. Thus, the assumption of constant channel over 2 OFDM-symbols for STBC is not restricting for the considered scenarios up to 300 km/h.

B.3 Effect of Channel Scenarios on Systems

As many parameters can influence performance, we only mention the most significant ones for each algorithm.

Concerning prefiltering, as CZF algorithm exploits the space-frequency diversity, the main parameters that influence performance is the channel correlation in space and frequency.

Concerning beamforming, its validity for different channel scenarios has been studied with the MSNR algorithm. It mainly depends on the value of the maximum eigenvalue of the estimated spatial autocorrelation matrix, as it represents the measure of the resulting SNR with beam formed. Fig. 16 presents optimistic results in a BRAN E-*ter* channel [26] with LOS (Rice factor $K = 100$). As expected, it can be observed that beamforming performs better with narrower angle spreads, as wider ones cause MAI and impose performance limit. The channel with $K = 100$ can be considered as a limit, i.e., a single path channel where a transmit beamforming gain of 3 dB is clearly observed.

Concerning STBC, the main parameter is channel correlation in space. The worst case is observed when the channel is totally correlated as the diversity is minimum, and performance is the same as SISO MC-CDMA one. The best performance is observed when the diversity is maximum, i.e., when there is no spatial correlation at both sides.

The influence of user's repartition and load is another parameter that is important, especially when considering beamforming.

Indeed, as MAI limits performance of MSNR and AoA algorithms, beamforming results generally improve significantly in non-full-load cases.

C. Proposed Strategy for Beyond-3G

Given the previous results, a beyond-3G communication system could select the best algorithm according to the environment. Note that a switch of antenna configuration at BS is also required to accept the studied beamforming algorithm with lower antenna spacing. We confirmed that CZF prefiltering can only be applied in indoor and low-speed scenarios, and presents the best results if instantaneous CSI is available at BS. The quality of estimation at BS, and the channel correlation between estimates and their use in the CZF algorithm will be a key factor on performance. Thus, this scheme is suitable for indoor scenarios and allows transferring the most computational complexity from MT to BS. We verified that the beamforming algorithms presented are really dependant of the spatial environment, but not of the quality of CSI at BS. These schemes are suitable for high-speed MT, in particular in outdoor scenarios with LOS, and when the number of TX-antennas is sufficient compared to the number of users. Suburban environments with large cells often verify such conditions. While beamforming prefers low angle-spread and high spatial correlations, STBC algorithms show their great interest when spatial correlation is low, and do not require CSI at BS. This scheme presents good results in all scenarios as the worst case corresponds to MISO performance. Indoor environments, but also urban conditions, like outdoor non-LOS transmissions with higher speed MT, would allow high data-rates.

VII. CONCLUSION

The combination of multiple antennas and MC-CDMA has proven its efficiency for the downlink of the next generation mobile communications. The study of such systems in realistic scenarios is an additional step towards an optimized achievement. Considering several levels of channel knowledge at base-station and various impairments, performance trends have been drawn. Depending on the mobile terminal class, its number of antennas or complexity allowed, different available data-rates have been proposed, using three main algorithms developed within the European IST-MATRICE project. All presented schemes have a reasonable complexity at mobile terminal, and are compatible with a single-antenna device. A choice between these algorithms has been proposed depending on the environment. Many parameters affect performance, but a strategy for beyond-3G can be outlined as prefiltering for indoor and pedestrian microcell environments, beamforming for suburban macrocells including high-speed train, and space-time coding for urban conditions with moderate to high speeds.

ACKNOWLEDGMENTS

The work presented in this paper was partly supported by the European FP5 IST project **MATRICE** (**M**ulticarrier-CDMA **TR**ansmission Techniques for **I**ntegrated Broadband **CE**llular Systems) [2] and partly by Spanish National Project TIC2003-09061-C03-01.

REFERENCES

[1] T. Ojanperä and R. Prasad, *Wideband CDMA for Third Generation Mobile Communications*, Artech House Publishers, 1998.
[2] IST MATRICE project, http://www.ist-matrice.org.
[3] IST 4MORE project, http://www.ist-4more.org.
[4] S. Abeta, H. Atarashi, and M. Sawahashi, "Forward link capacity of coherent DS-CDMA and MC-CDMA broadband packet wireless access in a multi-cell environment," in *Proc. IEEE VTC 2000 Fall*, 2000.
[5] S. Hara and R. Prasad, "Overview of multicarrier CDMA," *IEEE Commun. Mag.*, vol. 35, pp. 126–133, Dec. 1997.
[6] F. Portier *et al.*, "Performance comparison of multi-user detectors for the downlink of a broadband MC-CDMA system," in *Proc. IST Mobile & Wireless Commun. Summit*, 2004.
[7] J.-M. Auffray, J.-Y. Baudais, and J.-F. Hélard, "STBC MC-CDMA systems: Comparison of MMSE single-user and multi-user detection schemes over rayleigh and MIMO METRA channels," *European Trans. Commun.*, vol. 15, pp. 275–281, 2004.
[8] A. F. Naguib, A. J. Paulraj, and T. Kailath, "Capacity improvement with basestation antenna arrays in cellular CDMA," *IEEE Trans. Veh. Technol.*, vol. 43, pp. 691–698, Aug. 1994.
[9] E. Telatar, "Capacity of multiantenna gaussian channels," *European Trans. Commun.*, vol. 10, Nov./Dec. 1999.
[10] G. J. Foschini and M. J. Gans, "On limits of wireless communications in a fading environment when using multiple antennas," *Wireless Pers. Commun.*, vol. 6, 1998.
[11] T. Sälzer and D. Mottier, "Transmit beamforming for SDMA in multicarrier CDMA downlink of a per subcarrier basis," in *Proc. IEEE Int. Conf. Telecommun. 2003*, Feb./Mar. 2003.
[12] C. K. Kim and Y. S. Cho, "Performance of a wireless MC-CDMA system with an antenna array in a fading channel: Reverse link," *IEEE Trans. Commun.*, vol. 48, Aug. 2000.
[13] B. R. Vojcic and W. M. Jang, "Transmitter precoding in synchronous multiuser communications," *IEEE Trans. Commun.*, vol. 46, Oct. 1998.
[14] T. Sälzer *et al.*, "Pre-filtering using antenna arrays for multiple access interference mitigation in multicarrier CDMA downlink," in *Proc. IST Mobile & Wireless Communications Summit*, 2003.
[15] A. Silva and A. Gameiro, "Transmit space-frequency prefiltering technique for downlink TDD MC-CDMA systems," in *Proc. IEEE VTC 2003 Fall*, 2003.
[16] I. Raos and S. Zazo, "Downlink MISO proposal with transmit beamforming and diversity gain for B3G MC-CDMA systems," in *Proc. IST Mobile & Wireless Commun. Summit*, 2004.
[17] S. Zazo and I. Raos, "Transmit beamforming design in wide angle spread scenarios for B3G MC-CDMA systems," in *Proc. IEEE SPAWC*, 2004.
[18] S. M. Alamouti, "A simple transmit diversity technique for wireless communications," *IEEE J. Select. Areas Commun.*, vol. 16, pp. 1451–1458, Oct. 1998.
[19] V. Tarokh, H. Jafarkhani, and A. R. Calderbank, "Space-time block coding for wireless communications: Performance results," *IEEE J. Select. Areas Commun.*, vol. 17, pp. 451–460, Mar. 1999.
[20] F. Portier *et al.*, "STBC MC-CDMA systems for indoor and outdoor scenarios," in *Proc. IEEE ISSSTA 2004*, 2004, pp. 555–559.
[21] F. Portier, J.-Y. Baudais, and J.-F. Hélard, "Performance of STBC MC-CDMA systems over outdoor realistic MIMO channels," in *Proc. IEEE VTC 2004 Fall*, vol. 4, 2004, pp. 2409–2413.
[22] S. Kaiser and K. Fazel, "A flexible spread-spectrum multi-carrier multiple-access system for multi-media applications," in *Proc. IEEE PIMRC'97*, 1997.
[23] H. Krim and M. Viberg, "Two decades of array signal processing research—the parametric approach," *IEEE Signal Processing Mag.*, vol. 13, pp. 67–94, July 1996.
[24] 3GPP2 TR 25.996, 2003-05, "Network spatial channel model for multiple input multiple output simulations (release 6)," 3GPP spatial channel AHG, SCM-134, Apr. 2003.
[25] J. Medbo and P. Schramm, "Channel models for HiperLAN2," ETSI BRAN document no. 3ERI085B, 1998."
[26] J. Ojala *et al.*, "On the propagation characteristics of the 5 GHz rooftop-to-rooftop meshed network," in *Proc. IST Mobile & Wireless Commun. Summit*, 2002.
[27] Public documents—deliverable D3.5 "physical layer reference simulation results," 2004, available at http://www.ist-matrice.org.

Fabrice Portier received the Dipl.-Ing. and the M.Sc. degrees from the National Institute of Applied Sciences (INSA), France, in 2002. He is currently working towards the Ph.D. degree in the Institute of Electronics and Telecommunications of Rennes. His current research interests include the study and optimisation of Multi-Antennas Multi-Carrier Spread-Spectrum systems, in particular in a beyond-3G high data-rate wireless context. He is involved in research projects about space-time coding and MIMO channel estimation.

Ivana Raos received the Dipl.-Ing. in 1999 and Advanced Studies Diploma in 2001 from School of Electrical Engineering, University of Belgrade and from Department of Signals Systems and Radiocommunications of Technical University of Madrid (UPM), respectively. She is currently pursuing the Ph.D. degree in this Department. Her research interests in digital signal processing area are HF, mobile communications, multicarrier modulations for single, and multiple users access. She is involved in research projects about HF communications, future mobile communication systems (4G), and WLAN.

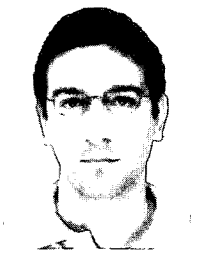

Adão Silva received his B.Sc. and M.Sc. degrees from the University of Aveiro, both in Electronics and Telecommunications, in 1999 and 2002, respectively. He is currently working towards the Ph.D. degree at the same university. He became an invited assistant professor in the Department of Electronics and Telecommunications of the University of Aveiro, and a researcher at the Instituto de Telecomunicações - Pólo de Aveiro. His main interests lie in signal processing techniques and space-time-frequency coding for wireless communications. His current research activities involve pre-equalization and space-time-frequency algorithms for the broadband component of 4G systems.

Jean-Yves Baudais received the M.Sc. degree and the Ph.D. degree in electrical engineering from the National Institute of Applied Sciences of Rennes (INSA), France, in 1997 and 2001, respectively. Since 2002, he has been working as CNRS researcher (French National Centre for Scientific Research) in the Institute of Electronics and Telecommunications of Rennes (IETR). Dr. Baudais was involved in several European and national research projects in the fields of mobile radio communications and power line transmissions. His general interests lie in the areas of signal processing and digital communications. Current research focuses on transmitter and receiver diversity techniques for multiuser and multicarrier communication including space-time coding.

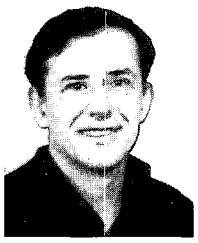

Jean-François Hélard received his Dipl.-Ing. and his Ph.D degree in Electronics and Signal Processing from the National Institute of Applied Sciences (INSA) of Rennes, France, in 1981 and 1992, respectively. In 1997, he joined INSA, where he is currently Professor and head of the group "Communications, Propagation and Radars" of the Rennes Institute for Electronics and Telecommunications (IETR). His present research interests lie in signal processing techniques for digital communications, as multicarrier modulation, spread spectrum, and multi-user communications. He is Senior Member IEEE, author or co-author of more than 60 technical papers in international scientific journals and conferences, and holds 12 European patents.

Atilio Gameiro received his Licenciatura (five years course) and his Ph.D. from the University of Aveiro in 1985 and 1993, respectively. He is currently a Professor in the Department of Electronics and Telecommunications of the University of Aveiro, and a researcher at the Instituto de Telecomunicações - Pólo de Aveiro, where he is head of group. His main interests lie in signal processing techniques for digital communications and communication protocols. Within this research line he has done work for optical and mobile communications, at theoretical and experimental levels, and has published over 100 technical papers in International Journals and conferences. His current research activities involve space-time-frequency algorithms for the broadband component of 4G systems and joint design of layers 1 and 2.

Santiago Zazo Bello is Telecom Engineer and Dr. Engineer by the Universidad Politecnica de Madrid (UPM) in 1990 and 1995, respectively. From 1991 to 1994, he was with the University of Valladolid and from 1995 to 1997 with the University Alfonso X El Sabio at Madrid. In 1998, he joined UPM as Associate Professor in Signal Theory and Communications. His main research activities are in the field of Signal Processing with applications to Audio, Communications, and Radar. Since 1990, he has participated in 15 projects with the Spanish industry and 4 European projects.